BAMS Article

# What Was the Bumpiest Flight Ever on NOAA's WP-3D Hurricane Hunter Aircraft?

Joshua B. Wadler,[a] Lauren Villafane,[b] Joseph J. Cione,[c] Kevin Adkins,[a] and George R. Alvey III[c,d]

**KEYWORDS:** Turbulence; Tropical cyclones; Aircraft observations

**ABSTRACT:** Motivated by experiencing extreme turbulence during a mission into Hurricane Ian (2022), this research develops a novel "bumpiness index" to objectively quantify the three-dimensional turbulence felt by scientists, pilots, and crew members on NOAA's WP-3D (hereafter P-3) Orion Hurricane Hunter aircraft missions. The bumpiness is derived using physics first principles and accounts for translational and rotational accelerations about an aircraft's three Cartesian axes. Since rotational motions are experienced differently depending on where someone is on a plane, the bumpiness index takes into account seat position. We then rank the bumpiest flights in recent history by gathering flight-level data from every tropical cyclone mission on the P-3 since 2004 when data needed from missions for this analysis became readily available as well as data from the infamous flights into Hurricanes Allen (1980) and Hugo (1989). Based on the maximum bumpiness value, the objective algorithm shows that the flight through Hurricane Hugo was the most turbulent ever with the flight into Hurricane Ian ranked second. The flight into Hurricane Hugo was unique because of the large accelerations associated with back–front motions, while the flight into Hurricane Ian was unique because of large accelerations associated with left–right motions. The next two bumpiest flights were in Hurricane Irma (2017) and Hurricane Sam (2021). Statistically, the bumpiest missions tend to be for stronger storms that will weaken in the subsequent 12 h. The largest values of bumpiness tend to be on the inner edge of the eyewall near a large gradient in radar reflectivity.

**SIGNIFICANCE STATEMENT:** After a turbulent mission on NOAA's WP-3D (P-3) Hurricane Hunter mission into Hurricane Ian from 2022, the crew wanted to know if it was the bumpiest mission ever. A bumpiness index was developed to characterize three-dimensional turbulence felt by crew on board and was used to rank all missions on the P-3 since 2004 and a couple of infamously turbulent older storms. Based on the bumpiness index, the mission into Hurricane Hugo was the bumpiest of all time with the mission in Hurricane Ian being the bumpiest since at least 2004. The bumpiness index developed in this study can be used for any aircraft.

DOI: 10.1175/BAMS-D-24-0065.1

*Corresponding author*: Joshua B. Wadler, wadlerj@erau.edu

Manuscript received 23 February 2024, in final form 26 February 2025, accepted 20 March 2025

**AFFILIATIONS:** [a] Embry-Riddle Aeronautical University, Daytona Beach, Florida; [b] National Weather Service Jacksonville Forecast Office, Jacksonville, Florida; [c] Hurricane Research Division, NOAA/Atlantic Oceanographic and Meteorological Laboratory, Miami, Florida; [d] University of Miami/Cooperative Institute for Marine and Atmospheric Studies, Miami, Florida

## 1. Introduction and motivation

On the first inbound leg into the eye of Hurricane Ian on 28 October 2022, the last mission before the storm made landfall on the southwest coast of Florida, onboard NOAA42 [one of two NOAA WP-3D (P-3) Hurricane Hunter aircraft], the aircraft experienced extreme turbulence. While turbulence on the P-3 is common, it is usually most predominate in the vertical direction. Unlike past missions, the mission into Hurricane Ian led to significant side-to-side motions that most crewmembers on the plane stated that they had not felt before. After this experience, a casual discussion broke out between the scientists on board and the resulting question: Was this the bumpiest hurricane flight on the P-3 in history?—led to this investigation.

The effect of atmospheric turbulence on aircraft has been studied extensively since it is the leading cause of commercial aircraft occupant injuries (e.g., Bass 2002; Tvaryanas 2003). Historically, turbulence monitoring has been done using pilot reports (PIREPs), which categorize the severity of the turbulence by the perceived intensity scales of "smooth" (also referred to as "null," "nil," or "neg"), "light," "moderate," "severe," or "extreme" (Federal Aviation Administration 2012). Due to PIREPs lacking quantitative scales, along with being inherently subjective, they can have substantial errors in reported intensity, position, and time (Schwartz 1996; Bass 2002; Sharman et al. 2006).

Currently, the International Civil Aviation Organization (ICAO) standard for aircraft turbulence reporting is eddy dissipation rate (EDR), which is the cube root of the dissipation rate of turbulent kinetic energy. EDR is a property of the atmosphere, and forecasts for EDR are produced by NOAA's Aviation Weather Center (AWC). EDR is aircraft independent for airframes of the same weight class. Separate forecasts of EDR are made for light (less than 15 500 pounds), medium (between 15 500 and 300 000 pounds), and heavy (greater than 300 000 pounds) aircraft. EDR is proportional to the vertical acceleration of the aircraft (MacCready 1964; Cornman et al. 1995) and can be calculated using winds measured at aircraft flight level (Sharman et al. 2014). A summary of other aircraft turbulence metrics can be found in Chan (1995).

While EDR quantifies the atmospheric turbulence, it does not necessarily quantify the human experience. Furthermore, EDR only accounts for the vertical component of turbulence. While this metric is widely accepted, we aim to develop a metric for bumpiness that accounts for all three dimensions of motion and considers the human experience, such that it is maximized when a person would say, "Wow, that was bumpy."

## 2. Data and methodology

All of the data needed to compute bumpiness for this investigation were obtained from 1-Hz flight-level data files stretching from 2004 to 2023. These files are in a netCDF format and are available on both the NOAA Hurricane Research Division (HRD) and Aircraft Operations Center (AOC) websites (see Open Research statement). On both data servers, raw data from 2012 or later typically have the extension "_A.nc," while automatic quality-controlled data

have the extension "_AC.nc." In some situations, the data system needed to be rebooted and the extensions "_BXC.nc" were used. Additionally, in some situations, meteorologists at AOC identified data that needed further quality control beyond the automated algorithm due to data spikes and dropouts. In cases where there was manual quality control, the data files were associated with "_AXC.nc" extension. If a file with manual quality control was available, that was always picked over the automated quality control. Of note, while data are available prior to 2004, they are ".1s" files that do not contain all the variables necessary to compute bumpiness. To date, there is no way to automatically obtain the necessary variables from the magnetic tapes in standard tape format that they are stored on (N. M. Dorst 2024, personal communication). However, we were able to obtain the data from two infamously turbulent flights (e.g., Dorst 2007; Marks et al. 2008) into Hurricanes Allen (1980) and Hugo (1989).

We attempted to use the P-3 flight-level data to compute EDR (Sharman et al. 2014) for direct comparison with our derived bumpiness index. However, the accurate computation of EDR requires significantly higher data frequency than 1 Hz. Files with 50-Hz data are also available and have the extension "_FST.nc." However, subjective evaluation of those data files led to questionable data quality, so they were not used. For example, the 50-Hz data from flight into Hurricane Ian showed similar side–side ($y$ direction) accelerations in the ferry to the storm as in the eyewall (not shown) which certainly did not occur. Zhang et al. (2011) showed that P-3 1-Hz flight-level data can sufficiently capture the turbulent characteristics of the flow (and implicitly for aircraft motion which is needed here).

The fundamental principle guiding the creation of the bumpiness index is that humans predominantly perceive accelerations and changes to accelerations (jerk) (Grant and Haycock 2008; de Winkel et al. 2020). For example, consider a common physics problem, the "elevator problem," where a person stands in an elevator. As the elevator begins to accelerate downward, the normal force between the person and the elevator decreases leading to a "weightless" feeling. When the elevator is traveling at a constant velocity, humans do not experience these sensations as the normal force is equal to as it would be standing on a nonmoving surface. As the elevator's acceleration changes to an upward acceleration as it comes to a stop, one would feel "scrunched" as the normal force between the person and the elevator increases. If the acceleration in the elevator changed rapidly, that would lead to a whiplash effect.

We define bumpiness using an aircraft-relative coordinate axes which follows a right-handed coordinate system. In this coordinate system, the $x$ axis aligns with the longitudinal axis of the aircraft (back–front), the $y$ axis aligns with the lateral axis of the aircraft (left–right), and the $z$ axis aligns with a vertical axis (up–down). As with any free body object, there are 3 degrees of freedom for both translational and rotational movements about the three axes (Fig. 1). Rotational motions about the $x$, $y$, and $z$ axes are called roll, pitch, and yaw, respectively, while translational motions about the $x$, $y$, and $z$ axes are called surge, sway, and heave, respectively.

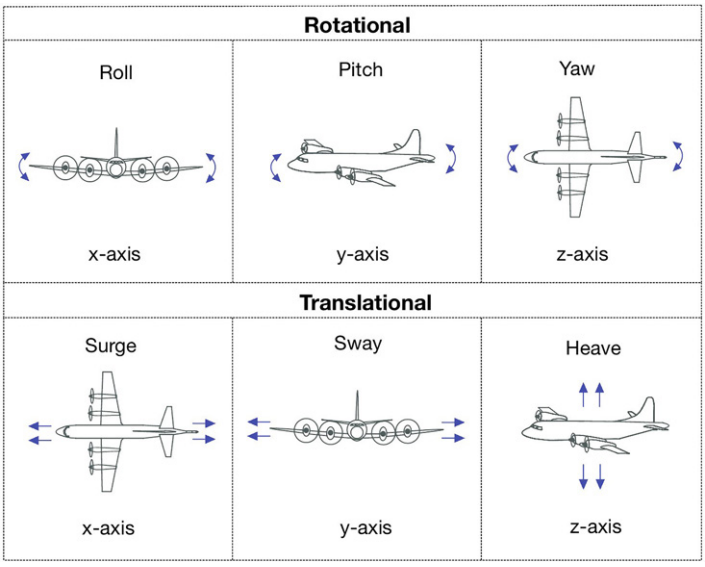


**Fig. 1. A description of the six different motions an aircraft can take.**

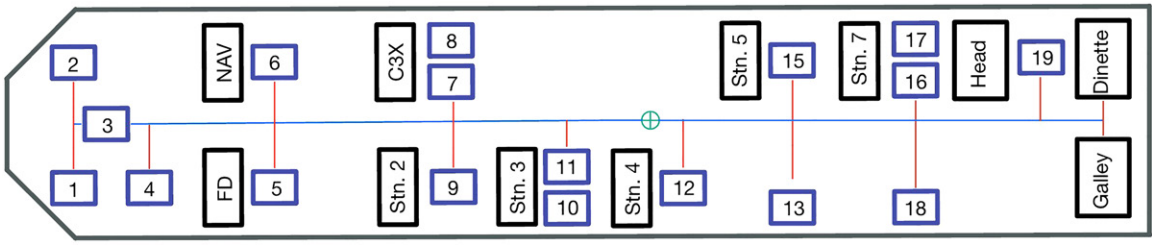


1. Pilot
2. Copilot
3. Flight Engineer
4. Station 1
5. Flight Director
6. Navigator
7. Station C3X
8. Station C3X
9. Station 2
10. Station 3
11. Station 3
12. Station 4
13. Project Seat
15. Station 5
16. Station 7
17. Station 7
18. Station 8
19. Dinette

⊕ Center of Gravity (CG)
X-distance from CG
Y-distance from X

**Fig. 2. A schematic layout of the P-3 seating chart. Note that no station 8 is drawn for seat 18 since there is no computer at that seat.**

***Building the bumpiness index.*** To build a bumpiness algorithm using flight-level data, we need to identify the magnitude of the motions that each person on the plane experiences. The shifts are different based on the individual's location relative to the center of gravity (axis of rotation). While everyone on the aircraft experiences the same translational motions, those farther from the center of gravity will experience stronger rotational motions than those closer to the center of gravity. For example, consider a rotating merry-go-round in a park. A person sitting at the center of the merry-go-round would feel the least amount of rotation while a person sitting at the edge would experience the greatest feeling of rotation. The center of gravity on the P-3 was obtained from a flight engineer and is located near the floor on the back corner of station 4 where the data technician sits (seat 12; see marking in Fig. 2). It is assumed that the center of gravity does not change significantly throughout the flight and from mission to mission which was confirmed by the flight engineer. There are typically 18 seats on the P-3. For consistency, we exclude seat 14 in Fig. 2 which appears on the standard P-3 seating chart but is not currently installed on the aircraft. Of note, seats can move up–down and side–side, but we measured from a standard location in front of a computer. Small changes to the seat locations should be insignificant (< 1% difference) to the bumpiness calculation. The derivation for the bumpiness of each seat is given in the appendix.

## 3. Results

To capture bumpiness in storms, we limit our dataset to only P-3 flights into tropical cyclones (TCs). To guarantee that the high bumpiness values are not associated with takeoff, landing, or the ferry, we further restrict application of our algorithm to when the P-3 is 15 min outside of takeoff or landing, when the P-3 is between 500- and 15 000-ft altitude [typical in-storm altitude is 2438 or 3048 m depending on if the Air Force WC-130 J (C-130) Hercules Hurricane Hunter planes are in the storm], and the current rate of altitude change is less than 1.52 m $s^{-1}$. We ensured that this does not eliminate times when the P-3 is flying pressure surfaces into strong TCs. While this altitude range can cover different types of turbulence, our goal in this research is to capture any turbulence experiences in storm conditions.

The classification is undertaken by considering the maximum 1-s bumpiness value from any point while in storm. Table 1 shows the top 20 flights for bumpiness in seat 1 (pilot). From this algorithm, the bumpiest flight was the Hurricane Hugo mission from 1989 with a bumpiness value of 7.86 m $s^{-2}$. During this mission, the turbulence was so bad that the P-3 lost an engine and had to orbit in the eye until finding a safe exit (Marks et al. 2008). The flight into Hurricane Ian, the mission that motivated this work, ranked second with a

bumpiness value of 6.04 m s$^{-2}$. From that seat, the flight into Hugo was 30.1% worse than in Hurricane Ian which was 34.2% higher than the third bumpiest flight which was from Hurricane Irma from 2017. Less separation exists from Irma to the fourth ranked storm, Hurricane Sam in 2021.

**Table 1. A ranking of the top 20 bumpiest P-3 flights from seat 1 in the aircraft. Storms with an "(EP)" are in the eastern Pacific basin. Mission IDs are given by the year, month, day, H, or I signifying NOAA42 or NOAA43, respectively; 1 or 2 indicating the first or second flight of the day with that aircraft.**

| Rank | Storm | Mission ID | Bumpiness (m s$^{-2}$) |
|---|---|---|---|
| 1 | HUGO | 19890915H1 | 7.86 |
| 2 | IAN | 20220928H1 | 6.04 |
| 3 | IRMA | 20170908H2 | 4.50 |
| 4 | SAM | 20210929H2 | 4.39 |
| 5 | LANE (EP) | 20180822H1 | 4.28 |
| 6 | FELIX | 20070902H1 | 4.27 |
| 7 | DORIAN | 20190830H2 | 4.08 |
| 8 | PATRICIA (EP) | 20151023I1 | 4.05 |
| 9 | RAFAEL | 20121015H1 | 4.02 |
| 10 | ALLEN | 19800806H1 | 3.94 |
| 11 | GONZALO | 20141017I1 | 3.90 |
| 12 | DORIAN | 20190904H1 | 3.71 |
| 13 | MICHAEL | 20181010H1 | 3.67 |
| 14 | CRISTOBAL | 20140826I1 | 3.64 |
| 15 | LAURA | 20200826H1 | 3.62 |
| 16 | TEDDY | 20200918I1 | 3.52 |
| 17 | DELTA | 20201009H1 | 3.51 |
| 18 | HENRI | 20210820H1 | 3.43 |
| 19 | KAREN | 20131004H1 | 3.40 |
| 20 | TEDDY | 20200917H1 | 3.40 |

A natural question is what happened during the flight into Hurricanes Hugo and Ian that made them so bumpy? Since the flight into Hugo is well documented and there are no raw horizontal acceleration measurements from earlier storms (see appendix), Fig. 3 shows the translational accelerations as well as the three rotational angle deviations over a 5-s span centered on the bumpiest moment of the Hurricane Ian flight. The P-3 was accelerating (or surging) forward during this time (Fig. 3a). The forward acceleration maximized at the time of maximum bumpiness. Thus, the magnitude of the jerk in the $x$ direction is maximized (the actual jerk is a minimum) at the time of maximum bumpiness. Over the 5-s span, the side–side motion (or sway; Fig. 3b) goes from accelerating toward the right at 0.5 m s$^{-2}$ to switching directions and accelerating toward the left by 3.5 m s$^{-2}$ and then back to accelerating to the right. Thus, the jerk in the $y$ direction is maximized 1 s after at the time of maximum bumpiness. The plane also switched from an upward acceleration (or heave) of 1 m s$^{-2}$ to a downward acceleration of 4 m s$^{-2}$ to an upward acceleration of 4 m s$^{-2}$ (the maximum in jerk was also 1 s after the time of maximum bumpiness).

In terms of rotational motions, over the same 5-s period, the roll angle changed from –14° to +5° to then +3°. Thus, the aircraft rotated in different directions over that 5-s period. The aircraft went from pitching up 0.5° to pitching down 6° to pitching down 2°. Note that the typical aircraft attitude during penetration is between +2° and +3° pitch. For yaw angle, the directional changes of the aircraft occurred over a much shorter period of time. Over the course of 3 s, the aircraft changed from a 68° heading to a 55° heading. Combined, all six of these changes in motion led to the second bumpiest moment on the P-3 in a TC. A remarkable feat of this mission was that after this P-3 and crew experienced this extreme bumpiness, it still made its way into the eye of Ian and released a small uncrewed aerial system (sUAS; e.g., Cione et al. 2020) called the Altius-600, which was the first time this particular aircraft was released into a TC.

With only values for seat 1 shown in Table 1, we show the breakdown of bumpiness values for all seats for the mission into Hurricane Ian in Table 2. Typically, scientists from the Hurricane Research Division of NOAA sit at seats 9, 10, and 11. The least bumpy location was seat 10 (typically the lead project scientist or radar scientist) with a value of 4.40 m s$^{-2}$, 36.2%

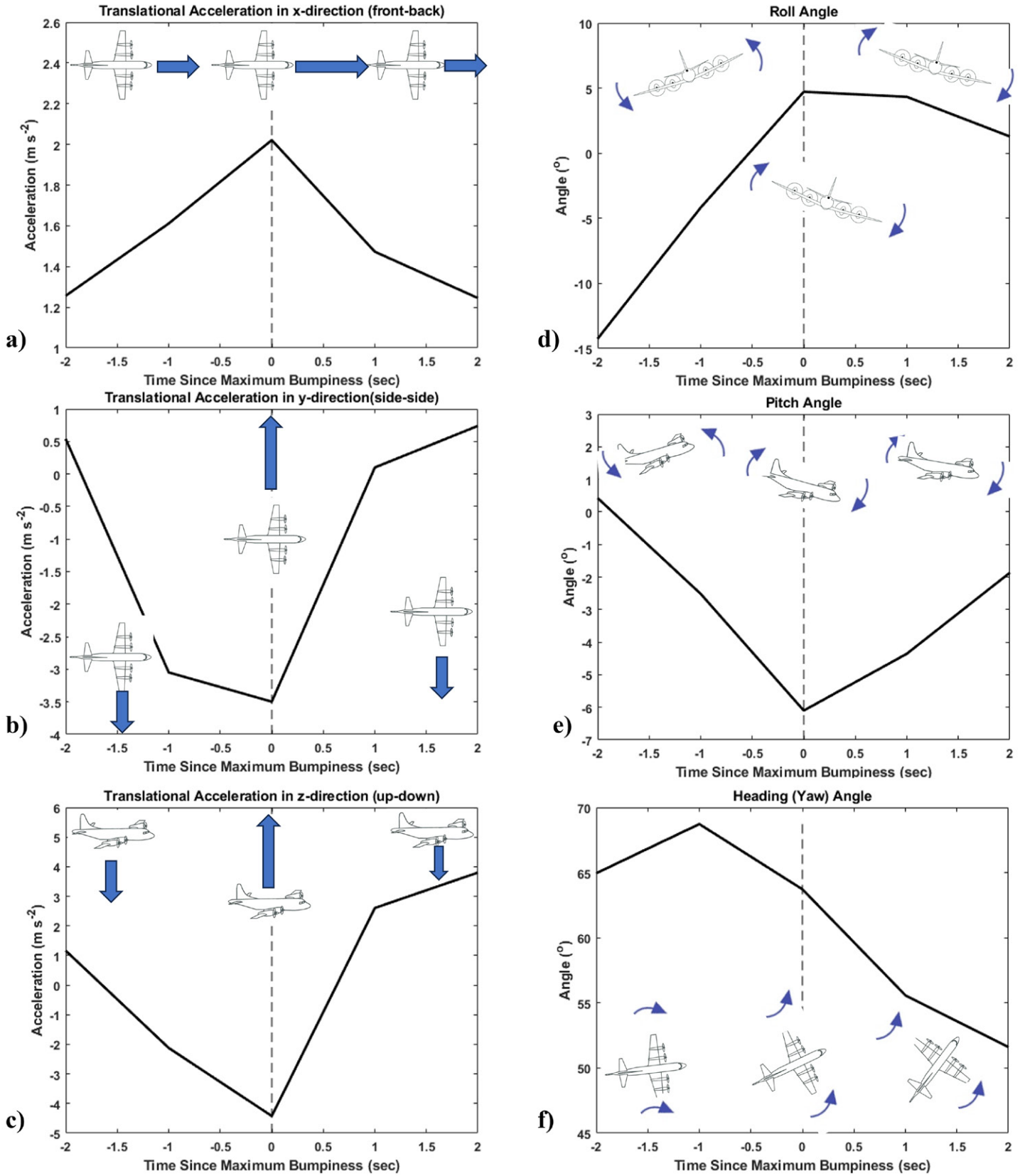


FIG. 3. Time series of translational accelerations in the (a) *x* direction (surge), (b) *y* direction (sway), and (c) *z* direction (heave) from 2 s before to 2 s after the bumpiest time during Hurricane Ian. (d)–(f) As in (a)–(c), but for time series of roll, pitch, and yaw angles, respectively. In each panel, the time of maximum bumpiness in outlined by a vertical dashed line. Additionally, the motion of the aircraft in each panel is outlined in schematics (not drawn to scale). Of note, to show the details in each panel, the range of *y* values is different in each plot.

less bumpy than the highest value which was for seat 2 (a bumpiness value of 6.13 m $s^{-2}$). Ironically, the first author of this manuscript was sitting at seat 10. The most bumpy seat was seat 2 (right pilot) with a value of 6.13 m $s^{-2}$.

The distribution of maximum bumpiness values for seat 1 (pilot), seat 11 (scientist), and seat 19 (a galley seat which is usually not occupied during penetration) for all flights is shown in Fig. 4a. As shown earlier, the Hurricane Hugo flight was the highest outlier with seat 1 having a bumpiness value of 7.86 m $s^{-2}$. The bumpiness values for seats 11 and 19 at the same time in that mission are 7.14 and 6.11 m $s^{-2}$, respectively. Since rotational motions are felt strongest at the seats farthest from the axis of rotation, the bumpiness values are typically highest in these locations. However, the median values of maximum bumpiness are comparable for each seat and range between 2.01 and 2.19 m $s^{-2}$, depending on the seat. The differences between seat 1 and seat 11 for each flight are shown in Fig. 4b. Most cases had negligible differences between the seats (indicating little rotational motion) with 57.9% of flights having less than |0.2| m $s^{-2}$ difference between seats. Negative differences indicate that bumpiness was higher in the center of the plane than the front as translational motions act in the opposite direction of rotational motions (vector subtraction). In this scenario, the highest bumpiness is typically realized at the back of the plane. The largest differences between seat 1 and seat 11 are positive, which is when rotational motions act in the same direction as the translational motions.

**Table 2. A comparison between the maximum values of bumpiness between the different seats on the P-3 during the mission into Hurricane Ian which ranked as the most bumpy flight since 2004 and the second bumpiest flight in history.**

| P-3 seat number | Maximum bumpiness value (m $s^{-2}$) |
|---|---|
| 1 | 6.04 |
| 2 | 6.13 |
| 3 | 6.02 |
| 4 | 5.87 |
| 5 | 5.52 |
| 6 | 5.68 |
| 7 | 5.03 |
| 8 | 5.08 |
| 9 | 4.79 |
| 10 | 4.4 |
| 11 | 4.46 |
| 12 | 4.45 |
| 13 | 4.54 |
| 15 | 4.45 |
| 16 | 4.53 |
| 17 | 4.51 |
| 18 | 4.59 |
| 19 | 4.55 |

For the top five bumpiest missions from Table 1, we explore the contributions of bumpiness from each aircraft-relative direction in Fig. 5. Note that in Fig. 5, the scales for each plot are different to highlight details in the trends. In the *x*-direction motions (back–front; Fig. 5a), the flight into Hurricane Hugo had substantially higher

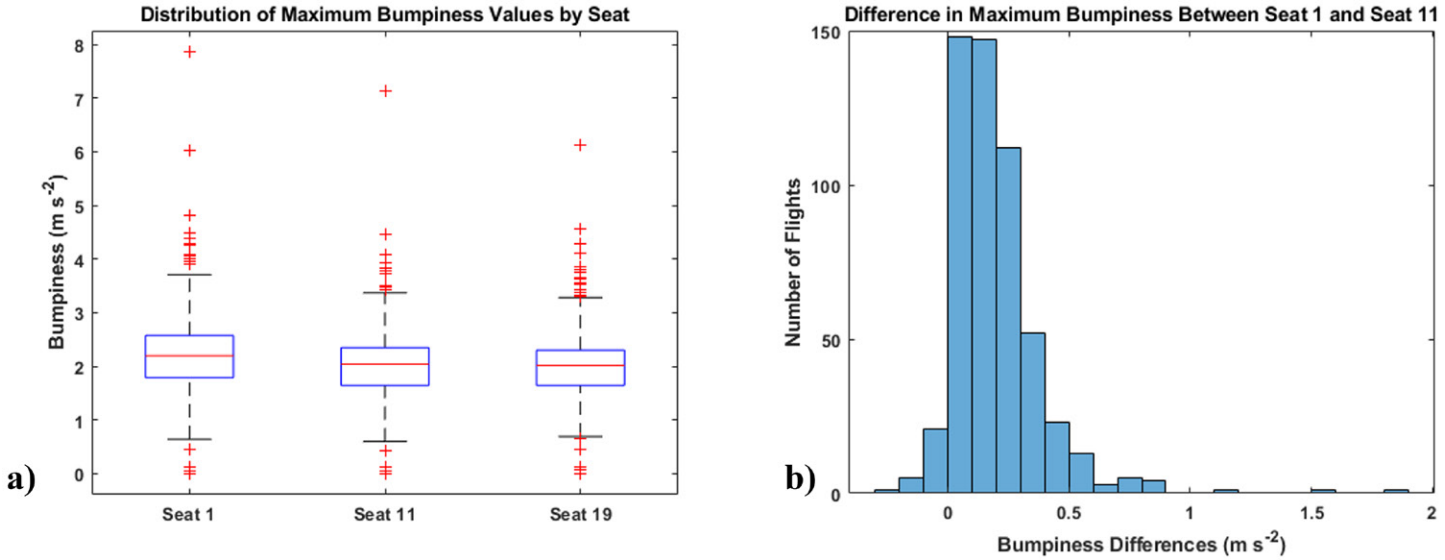


**Fig. 4. (a) Boxplot comparisons of the maximum values of bumpiness for seats 1, 11, and 19 on the P-3. (b) Histogram of the differences between the maximum bumpiness value for seat 1 and seat 11 for every mission.**

contribution to bumpiness for all seats than any other storm. For most seats, the flight into Hurricane Ian had the second highest contribution to *x*-direction motions except in the middle of the plane where the flight into Hurricane Sam had a greater amount of back–front bumpiness. In the *y*-direction motions (side–side; Fig. 5b), Hurricane Ian had the highest values of bumpiness for all the seats. The large differences in the bumpiness between the front and middle of the plane for Ian indicate the larger role of rotational motions over translational motions. Of note, in Fig. 5b, all of these missions show higher amounts of bumpiness in the front of the plane than in the rear of the plane. That is because the rotational motions are in the same direction as the translational motions such as the aircraft accelerates to the left and yaws to the left. These outlier scenarios in Fig. 5b (same as discussed for Fig. 4b) lead to particularly strong motions in the front of the aircraft. In the rear of the aircraft, the motion due to rotation is opposite the motion due to accelerating toward the left, canceling each other out. The strongest total vertical motion from the top five list is Hurricane Lane from 2018 (Fig. 5c) with flights into Hurricanes Hugo and Sam having comparable values. Of note, the highest overall bumpiness in the *z* direction in the dataset was from Hurricane Sam from 2021, but it was not at the time of maximum bumpiness (it occurred 6 s later). Interestingly, of all the flights in the top five, Hurricane Ian has the lowest or second lowest

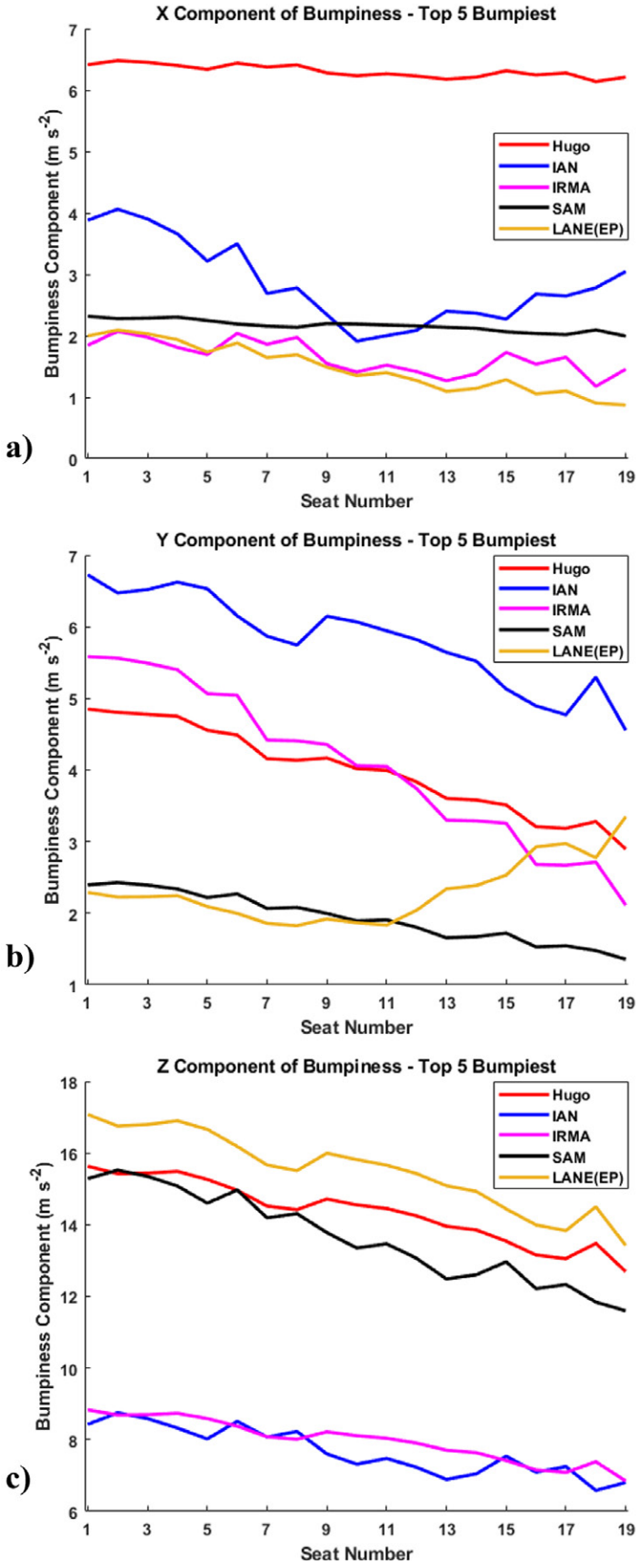


**FIG. 5. The (a) back–front (*x*) component (surge), (b) left–right (*y*) component (sway), and (c) up–down (*z*) component (heave) of bumpiness at the time of maximum bumpiness for each seat from the top five overall bumpiest flights in seat 1. Of note, the scale is different in each panel.**

vertical component of bumpiness. This confirms the subjective feeling from the scientists on the plane that the side–side motions were particularly strong. Even though the total bumpiness in the *x* and *y* directions is lower than in the vertical, high amounts of changes of motion in these directions are strongly felt by those on board.

To try to make an objective verification to the bumpiness index, an email was sent out to scientists at the HRD of NOAA (typical science crew on the aircraft) for which flights they believe were the bumpiest they had been on. A list of the responses is in Table 3. Unfortunately, a number of the storms put forth were prior to 2004, which predates the usable database for the bumpiest calculation. Interestingly, for every mission reported, that flight appeared in the top 20 bumpiest flights (according to seat 1 in Table 1) or a different mission into that same storm was objectively ranked in the top 20. The highest ranked storm to not be mentioned in the subjective list is Raphael from 2012 at number 9, but the crew manifest from the mission shows that no scientists from HRD were on board that mission.

To help flight crew potentially prepare for turbulent missions, a natural question is whether there are storm or environmental characteristics that are associated with high levels of bumpiness. To address this, we analyzed data from the Statistical Hurricane Intensity Prediction Scheme (SHIPS; DeMaria et al. 2005) developmental dataset which has output in 6-h intervals. The SHIPS output was matched to each flight using the closest output to the midpoint time of each flight. There is a negative correlation ($r = -0.19$, where $r$ is the Pearson correlation coefficient) between bumpiness and intensity change in the subsequent 12 h (Fig. 6a). Thus, while there are only limited number of cases, storms that will weaken have a higher chance of being bumpy than storms that will strengthen. Interestingly, the correlation with future intensity change is stronger than with current intensity change (Fig. 6d) or the difference in intensity between 6 h in the future and 6 h in the past. The highest correlation with bumpiness is current TC intensity (Fig. 6b) with an $r = 0.45$, indicating that stronger storms tend to be bumpier than weaker storms. Combined with Fig. 6a, this implies that strong storms near the end of an intensification cycle tend to be

**Table 3. A chronological list of storms subjectively identified by scientists at the HRD of NOAA to be the bumpiest they have been on along with how that storm was ranked by the bumpiness algorithm in Table 1.**

| Storm name | Flight ID | Result |
|---|---|---|
| Allen | 19800805H1 | No data |
| Allen | 19800806H1 | Number 10 |
| Hugo | 19890915H1 | Number 1 |
| Irene | 19810926H1 | No data |
| Emily | 19870922H1 | No data |
| Emily | 19870922I1 | No data |
| Claudette | 19910908I1 | No data |
| Irene | 19991015H1 | No data |
| Felix | 20070902H1 | Number 6 |
| Cristobal | 20140826I1 | Number 14 |
| Patricia | 20151023I1 | Number 8 |
| Irma | 20170908H1 | A different mission into this storm was ranked number 3 |
| Lane | 20180822H1 | Number 5 |
| Michael | 20181009H1 | A different mission into this storm was ranked number 13 |
| Michael | 20181010H1 | Number 13 |
| Dorian | 20190901H1 | Multiple different mission into this storm were ranked numbers 7 and 12 |
| Sam | 20210929H2 | Number 4 |
| Ian | 20220928H1 | Number 2 |

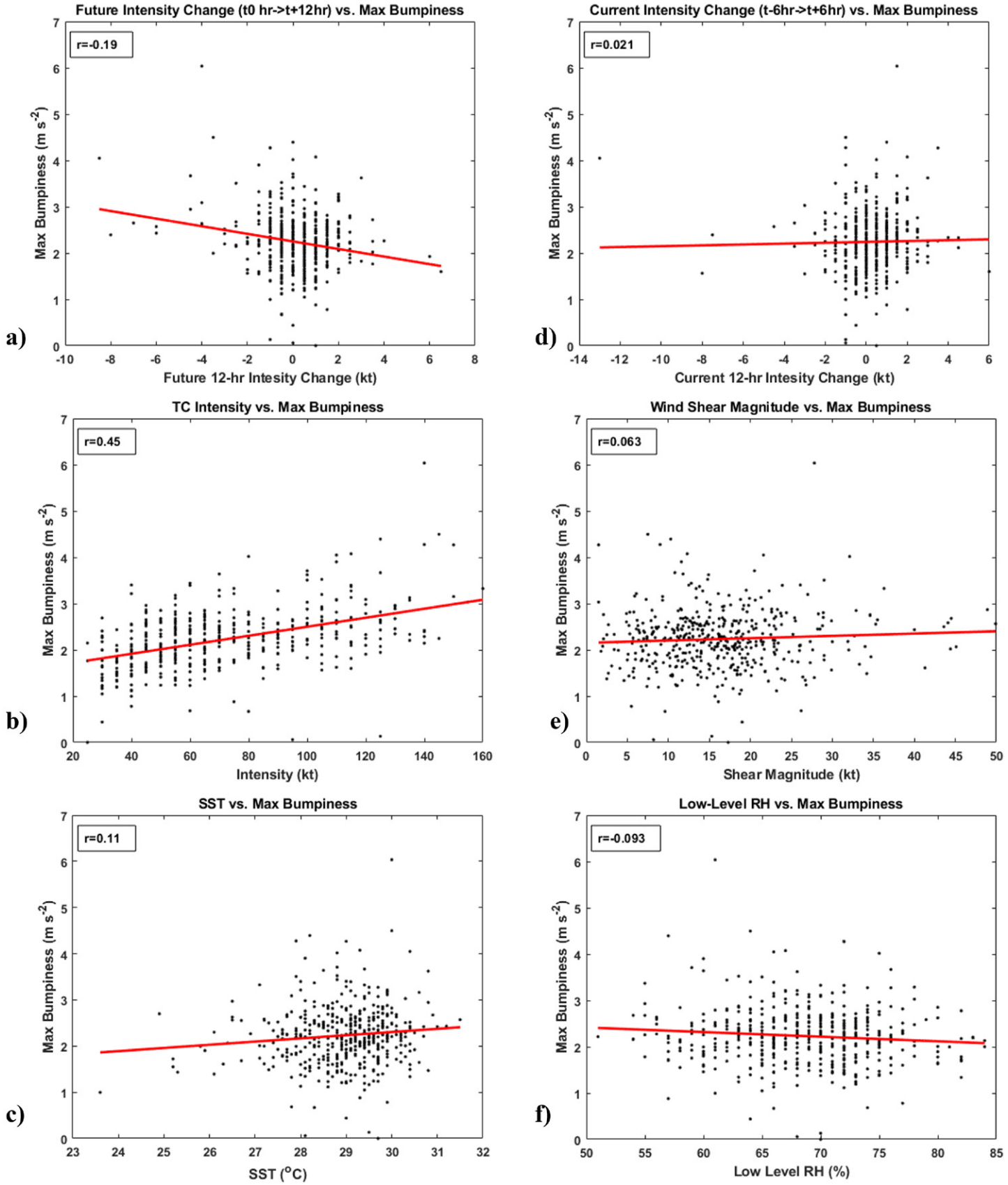


FIG. 6. Comparison of maximum bumpiness in seat 1 from each flight with (a) future 12-h intensity change, (b) current 12-h intensity change rate, (c) current storm intensity, (d) deep-layer wind shear magnitude, (e) sea surface temperature, and (f) low-level relative humidity. The Pearson correlation coefficient *r* and linear best-fit line are shown in each panel. Note that due to the time gap, data from Hurricanes Hugo and Allen are not included in this figure.

the bumpiest. None of the environmental variables, such as deep-layer wind shear magnitude ($r = 0.063$; Fig. 6e), sea surface temperature ($r = 0.11$; Fig. 6c), or low-level [850–500 mb (1 mb = 1hPa)] area-averaged relative humidity ($r = -0.093$; Fig. 6f), had strong correlations with maximum bumpiness. There is also a weak correlation between aircraft altitude and maximum bumpiness ($r = -0.096$; not shown) because the P-3 typically only flies between 2438 or 3048 m and does not experience the different turbulent kinetic energy values characteristic of different altitudes (e.g., Lorsolo et al. 2010).

With many environmental factors ruled out, we also investigate if there are trends in bumpiness over time. Recent work has shown that there will generally be more clear-air turbulence in a changing climate (e.g., Storer et al. 2017), so we investigated if flights have become bumpier on the P-3 over time. Overall, there has been some trend (again, albeit a relatively small sample size) toward bumpier flights since 2004 (Fig. 7a), with an $r$ value of 0.28, but there has not been a significant shift in the distributions over time. Potentially, the trends are due to changes to the P-3 airframe and/or addition of external pods that could make the aircraft more susceptible to slight changes in aerodynamic forces. The bumpiest month for missions tends to be September (Fig. 7b), but there may be a sampling bias due to more missions occurring during September with it being the climatological peak for TC activity in the Atlantic basin (NOAA 2024). There have been 226 missions in the month of September since 2004 which is significantly higher than the second most flown month of August with 168 missions.

To further examine what precipitation features are associated with high values of bumpiness, we linked the aircraft location at time of maximum bumpiness to ground-based radar. While most flights were beyond the range of a ground-based radar site, Fig. 8 shows a radar image at time of maximum bumpiness for Hurricane Ian (ranked number 2), Hurricane Dorian (ranked number 7), Hurricane Michael (ranked number 13), and Hurricane Delta (ranked number 17). In the first three cases, the P-3 was on the inner edge of the eyewall near large reflectivity gradients and experienced enhanced horizontal motions (not shown). The bowing or notch-like reflectivity features (sometimes called "fingers" or "scallops") near and upstream of the P-3 may be associated with misovorticies, which have previously been identified in intense hurricanes within regions of strong horizontal shear instabilities (e.g., Aberson et al. 2006; Marks et al. 2008). Spectrum width (SW) values in excess of 4 m $s^{-1}$

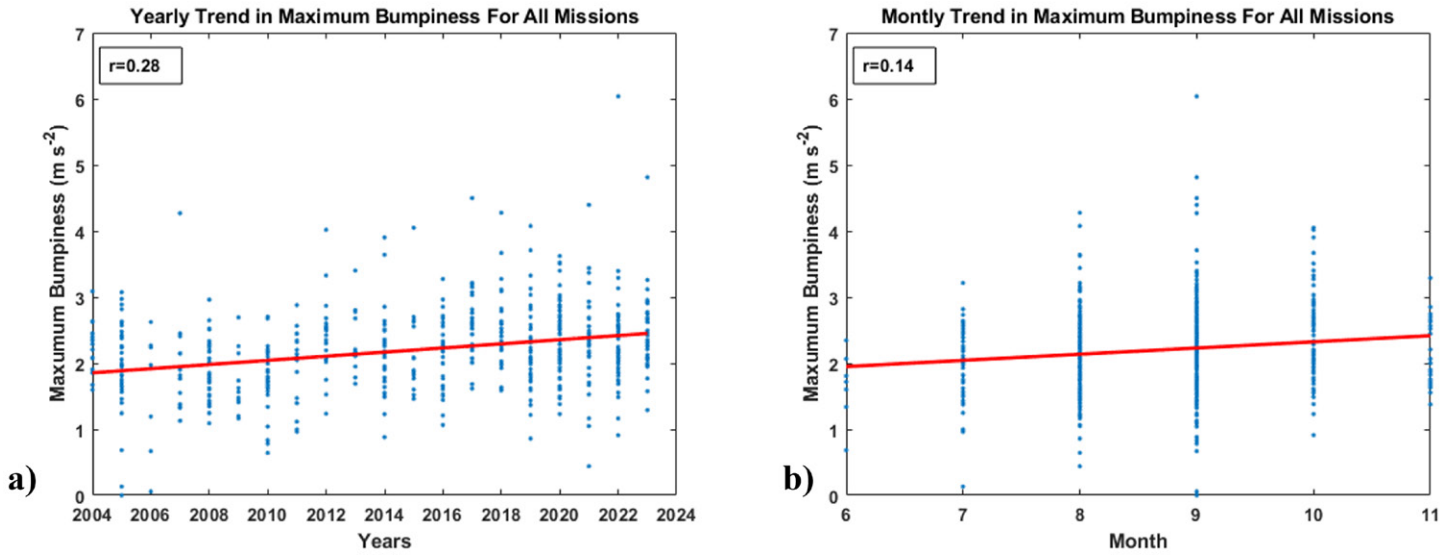


**Fig. 7. Scatterplots of the maximum bumpiness for seat 1 in each flight grouped by (a) year and (b) month. The Pearson correlation coefficient $r$ and linear best-fit line are shown in each panel. Note that due to the time gap, data from Hurricanes Hugo and Allen are not included in this figure.**

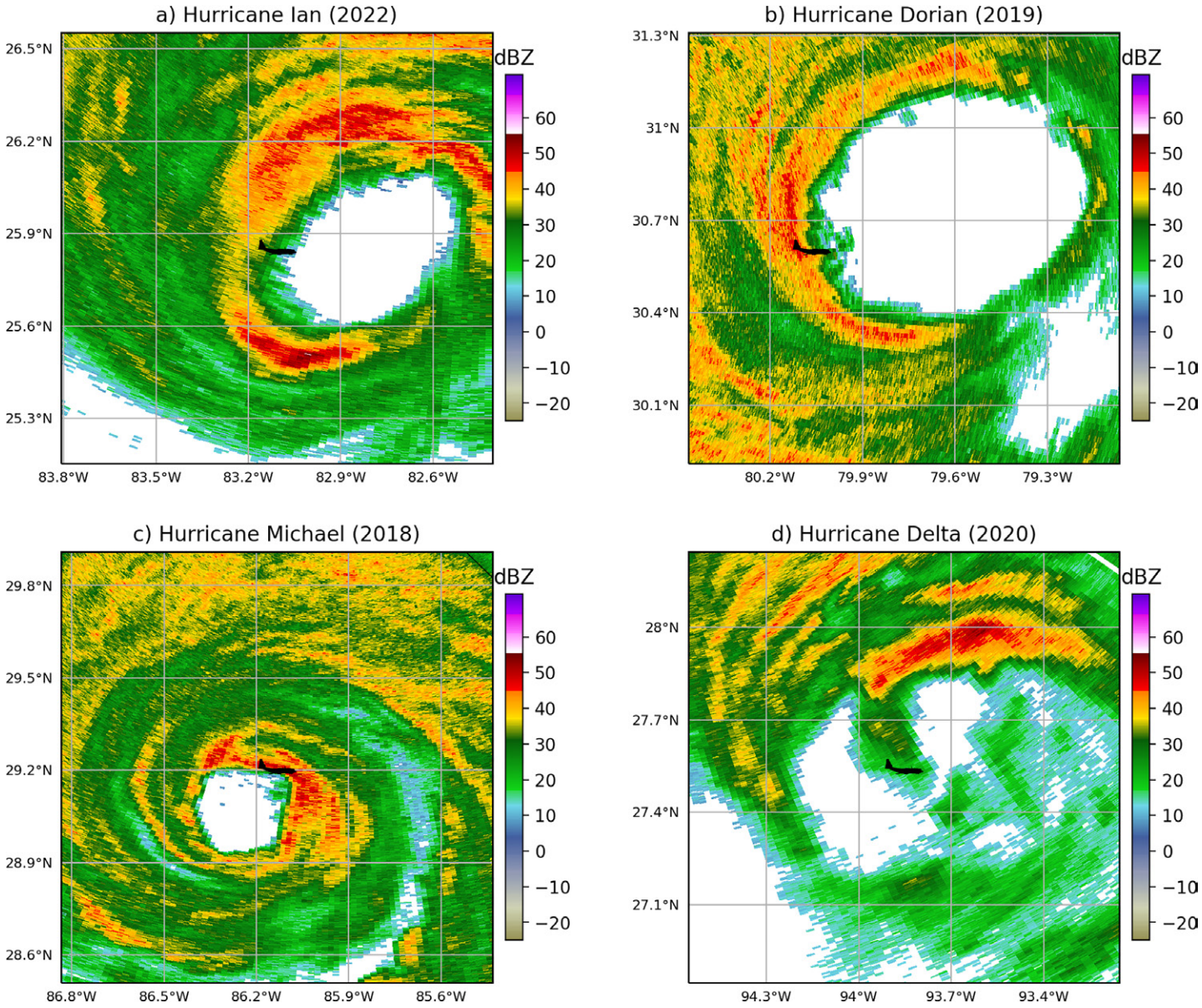


**FIG. 8. WSR-88D radar reflectivity at 0.5° elevation along with air airplane icon noting the location of the P-3 at time of maximum bumpiness during missions into (a) Hurricane Ian from KTBW, Tampa, Florida, at 1014 UTC 28 Sep 2022; (b) Hurricane Dorian from KJAX, Jacksonville, Florida, at 0042 UTC 5 Sep 2019; (c) Hurricane Michael from KEVX, Eglin Air Force Base, Florida, at 1233 UTC 10 Oct 2018; and (d) Hurricane Delta from KHGX, Houston, Texas, at 1239 UTC 9 Oct 2020.**

generally provide an indication of significant turbulence that may be hazardous to aircraft (Lee 1977; Evans 1985); however, it is important to note that SW is measurement of not only turbulence but also wind shear (Melnikov and Doviak 2009). In all three cases wherein observable SW of the TC core is within range of the ground radar (Dorian, Ian, Michael), the maxima (in excess of 10 m $s^{-1}$) in SW were generally in close proximity to the aircraft (< 10 km). In Hurricane Delta, the storm was interacting with shear and dry air (Cangialosi and Berg 2021), and the bumpiness was associated with a stronger vertical component of turbulence than in Ian, Dorian, and Michael (not shown). A thorough study of storm characteristics that lead to enhanced bumpiness is a topic of future research.

## 4. Summary

Motivated by the scary ride into Hurricane Ian on 28 October 2022, we developed an algorithm to define bumpiness experienced on an aircraft (or any free-motion object such as

a boat) and evaluated it for each seat on the NOAA P-3 Hurricane Hunter flights between 2004 and 2023 using 1-Hz flight-level data as well as for missions into Hurricanes Allen (1980) and Hugo (1989). The bumpiness experienced is not necessarily a property of atmospheric turbulence, like the commonly used EDR. Instead, the bumpiness algorithm developed is designed to show what humans feel and is applicable to any aircraft. Thus, as examples, the algorithm presented here may be transferred to pilots flying in and near similar wind shear zones associated with nonsevere and severe thunderstorms as well as clear-air turbulence associated with mountain waves and jet streams. The bumpiness index in this manuscript accounts for accelerations and jerks due to rotational and translational motions. Since each seat is at a different place relative to the center of gravity, the bumpiness due to aircraft rotations (and hence the overall bumpiness) varies between each seat on the plane.

Overall, the bumpiest singular moment on any mission was the flight into Hurricane Hugo with a value for the pilot seat of 7.86 m $s^{-2}$, 30.1% higher than the second bumpiest moment into Hurricane Ian. During Hurricane Ian, the pilot seat was also 36.2% more bumpy than the least bumpy seat which was for a scientist (the lead author of this manuscript) in seat 10. The flight into Hurricane Hugo was dominated by both front–back and up–down motions. Consistent with the subjective experiences of those on board, the bumpiness experienced in Ian was predominately associated with horizontal (particularly side to side) motions, which are more uncommon than vertical accelerations. Of all the missions in the top five, the mission into Hugo experienced the highest amount of bumpiness front–back motions, while the mission into Ian experienced the highest amount of bumpiness from left–right motions. The flight with the largest vertical component of bumpiness at the time of maximum bumpiness was Hurricane Lane (2018). The biggest recorded vertical bump, regardless of the overall bumpiness value, was in Hurricane Sam (2020).

There are widespread possible applications to the bumpiness index. It can be related to the safety and decision-making of crew on board all types of aircraft, not just the NOAA P-3. Future work is to further determine storm characteristics, particularly from the onboard lower fuselage multimode radar (MMR) which is used in real time for situational awareness. Future work should also evaluate the perception of the severity of the bumpiness as well as the impairment of cognitive function under bumpy conditions so that we can define a baseline for crew effectiveness and safety. Last, this work ranked missions based on the maximum 1-s bumpiness. Future work should consider a ranking based on a cumulative effect of bumpiness to develop a queasiness index.

**Acknowledgments.** This work is generously supported by the ERAU Faculty Innovative Research in Science and Technology (FIRST) and the Faculty Research Development Program. We sincerely thank the scientists and crew of the Aircraft Operations Center for flying through these turbulent storms in order to collect critical data that improve forecasts that help the American public. We are also thankful for Rich Henning and Nick Underwood from the Aircraft Operations Center for helping us find and understand the flight-level data files. We thank Neal Dorst for obtaining data from Hurricanes Allen and Hugo for this project. The comments from three anonymous reviewers and Editor Dr. Chris Landsea greatly helped improve the quality of the manuscript.

**Data availability statement.** All of the flight-level data files are archived on NOAA servers at the Atlantic Oceanographic and Meteorological Laboratory (https://www.aoml.noaa.gov/data-products/#hurricanedata) and at the Aircraft Operations Center (https://seb.omao.noaa.gov/pub/acdata/).

## APPENDIX

## Building the Bumpiness Algorithm

We measured the distance from the center of gravity to the center of the cushion of each seat, and these distances are given in Table A1.

We first use the pitch, roll, and yaw angles to compute the motion experienced by each seat from its initial aircraft-relative position. It is assumed that the airframe is a rigid body and does not flex during flight such that the distances in Table A1 remain constant. Since the distance to the center of gravity determines how much rotational motion a person experiences, a distance traveled due to rotational motions in $x$, $y$, and $z$ ($dx_R$, $dx_R$, $dz_R$) is obtained by multiplying a rotation matrix given by Eq. (A1) by the initial distances from the center of gravity.

The total motion:

$$\begin{bmatrix} dx_R \\ dy_R \\ dz_R \end{bmatrix} = \mathbf{R} \begin{bmatrix} dx_0(s) \\ dy_0(s) \\ dz_o(s) \end{bmatrix}, \tag{A1}$$

where the rotation matrix is given by

$$\mathbf{R} = R_Z(\psi)R_y(\theta)R_x(\varphi) = \begin{bmatrix} \cos(\psi)\cos(\theta) & \cos(\psi)\sin(\theta)\sin(\varphi)-\sin(\psi)\cos(\varphi) & \cos(\psi)\sin(\theta)\cos(\varphi)+\sin(\psi)\sin(\varphi) \\ \sin(\psi)\cos(\theta) & \sin(\psi)\sin(\theta)\sin(\varphi)+\cos(\psi)\cos(\varphi) & \sin(\psi)\sin(\theta)\cos(\varphi)-\cos(\psi)\sin(\varphi) \\ -\sin(\theta) & \cos(\theta)\sin(\varphi) & \cos(\theta)\cos(\varphi) \end{bmatrix}, \tag{A2}$$

where $\psi$ is the yaw angle, $\theta$ is the pitch angle, and $\varphi$ is the roll angle. Of note, the three-dimensional rotation matrix used in this study [Eq. (A2)] is the matrix multiplication of the rotation matrices from yaw rotations, pitch rotations, and roll rotations. The matrix multiplication implies a temporal component to the motions, and a different ordering of the matrix multiplication of the individual rotation matrices for each rotation angle can yield different results. With the difficulty in obtaining a true yaw angle, in this study, we use aircraft heading angle as yaw angle. Since the bumpiness algorithm relies on changes to angles (see below) for accelerations and jerk calculations, heading angle is a reliable alternative to yaw angle and is a more widely measured quantity.

The 1-Hz P-3 flight-level data have been used in multiple studies (e.g., Jorgensen et al. 1985; Eastin et al. 2005a,b; Zhang et al. 2011; Aberson et al. 2017; Martinez et al. 2017; Wunsch and Didlake 2018; Pincus et al. 2021) and are obtained by applying multiple filters to the high-resolution 50-Hz data which are documented by Leise and Masters (2013) and summarized here. Prior to sampling at the high frequency rate, data are prefiltered with a four-pole Butterworth filter. Next, to obtain the 10-Hz rate (a middle step), data are "box-car" averaged and subsampled. Lastly, a 20-coefficient triangular filter centered on the data point is applied to obtain 1-Hz data. As discussed in Zhang et al. (2011), who used the 1-Hz data to study the turbulent nature of hurricane eyewalls, the 1-Hz P-3 wind

**Table A1. Distance (m) from the center of gravity to the cushion of each seat on the P-3.**

| Seat | *Dx* (m) | *Dy* (m) | *Dz* (m) |
|---|---|---|---|
| 1 | 9.4996 | −0.4064 | 0.7112 |
| 2 | 9.4996 | 0.9398 | 0.7112 |
| 3 | 9.0424 | 0.4572 | 0.7112 |
| 4 | 8.4328 | −0.4064 | 0.7112 |
| 5 | 6.35 | −0.8128 | 0.5334 |
| 6 | 6.4008 | 1.2192 | 0.5334 |
| 7 | 2.7178 | 0.8636 | 0.5334 |
| 8 | 2.7178 | 1.524 | 0.5334 |
| 9 | 2.1844 | −0.889 | 0.5334 |
| 10 | 0.4064 | −1.3716 | 0.5334 |
| 11 | 0.4064 | −0.7112 | 0.5334 |
| 12 | −1.4224 | −0.9906 | 0.5334 |
| 13 | −4.0386 | −1.3716 | 0.5334 |
| 14 | −4.0386 | −0.7112 | 0.5334 |
| 15 | −4.0386 | 1.3462 | 0.5334 |
| 16 | −7.4676 | 0.8636 | 0.5334 |
| 17 | −7.4676 | 1.524 | 0.5334 |
| 18 | −7.4676 | −1.27 | 0.5334 |
| 19 | −10.7696 | 0.9906 | 0.5334 |

velocity data are able measure turbulent eddies up to 200 m, based on the Nyquist frequency of 0.5 Hz.

Using the 1-Hz flight-level data for the three rotational angles, a $dx_R$, $dx_R$, and $dz_R$ value is associated with each of the 18 seats. Since, as stated earlier, the algorithm for bumpiness requires the acceleration and jerk of motions, we take a numerical second derivative of the displacements to obtain accelerations and a numerical third derivative of the displacements to obtain jerks. We tested various degrees of accuracy for the numerical derivatives to balance numerical stability with accuracy. A comparison between the derivatives for seat 1 during the mission into Hurricane Ian that ranked the second bumpiest in the dataset is given in Fig. A1. This flight was chosen for the comparisons due to the need of the algorithm to resolve large accelerations. All of the derivatives are able to capture the peak in accelerations, which occurs at 14 235 s into the file. The difference between the eighth-order accurate derivative and the sixth-order accurate derivative at that time is 0.0061 m $s^{-2}$. In contrast, the difference between the sixth-order accurate and fourth-order accurate derivative is 0.029 m $s^{-2}$, and the difference between the fourth-order accurate and second-order accurate derivative is 0.149 m $s^{-2}$. The eighth-order derivative, which includes information from 4 s before the time of interest to 4 s after, was able to capture the large acceleration experienced in the eyewall, and the differences between the eighth-order and sixth-order derivatives converge. Thus, for all derivatives in this study, we utilize an eighth-order central difference scheme. Since the high accuracy scheme can lead to numerical instability, there is the possibility of small errors in the flight-level data causing significant errors in the calculation. Additionally, the derivatives make the signal more sensitive to aliasing near the Nyquist frequency which is 0.5 Hz. We noticed some of these cases with obvious errors where the bumpiness was an order of magnitude higher than any other storm (only occurred seven times and all were in the earliest 2 years of the dataset) and manually removed them.

With the rotational motions defined, the accelerometers on the P-3 were used to observe the translational motions. In the flight-level data files, accelerometers report the total accelerations in the *x*, *y*, and *z* planes. However, they are only located in one area of the plane and not at the center of gravity. Thus, their measurements contain contributions from translational and rotational motions. To obtain the purely translational accelerations, we measured the distance of the sensors to the center of gravity which are –1.524, 0.8636, and 0.1524 m in the *x*-, *y*-, and *z*-coordinate system, respectively (they are in front of station 5, fairly close to the center of gravity). The contribution of rotational motions based on the location of the accelerometers is computed in the same manner as for each seat using Eqs. (A1) and (A2) and is subtracted from the reported accelerations. As with rotational motions, the jerk due to translational motions is computed using an eighth-order accurate numerical derivative.

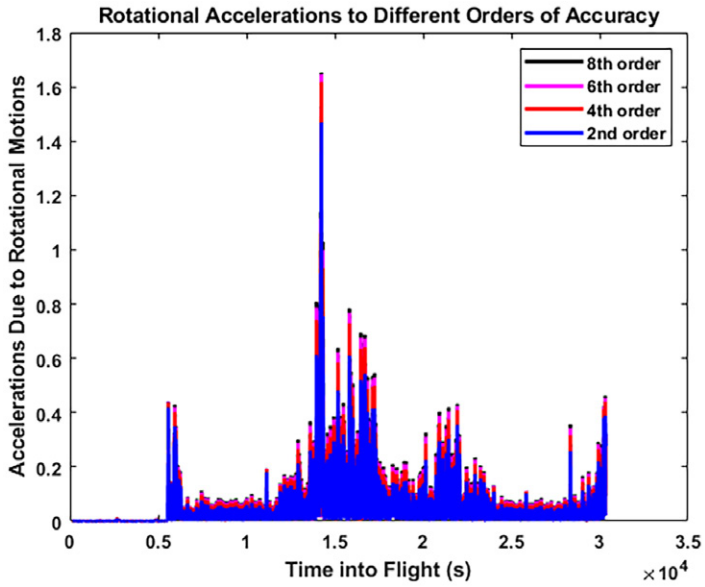


**Fig. A1. A comparison between the total accelerations due to rotational motions in seat 1 (pilot) of the P-3 using derivatives of different orders of accuracy.**

It is worth noting that having an accelerometer recording at each seat would eliminate the need for a rotation matrix as the instrument would report the combined effect of the rotational and translational components of the motion. The reported acceleration values at each seat would only need to be numerically differentiated to obtain a bumpiness value.

Accelerometers on board only report three-dimensional data since 2012. Prior to that year, the netCDF files have a different naming convention "_RC.nc" instead of "AC_.nc," with different variable names. Between 2004 and 2012, vertical acceleration (heave) is reported by the accelerometer but not the horizontal components of acceleration. To obtain the horizontal accelerations (surge and away) in cases prior to 2012, we use the aircraft velocity, which is reported in its zonal and meridional components. Since the velocity data can be noisy, the raw velocity measurements were smoothed by a 3-s moving mean. While this provides additional filtering to data prior to 2012, it was necessary to smooth out subjectively determined erroneous motions from the velocity data in regions where the flight was expected to be smooth. To obtain *x* accelerations (or surge; in the direction of aircraft motion), we use a dot-product projection of the aircraft velocity from one time step to the prior time step. The dot-product projection gives the component of the aircraft velocity that is parallel to the velocity at the previous time step. A derivative of the parallel velocity component gives the translational acceleration in the *x* direction. The difference between the total aircraft velocity and the parallel component of the velocity is the perpendicular component of the velocity (or sway). If we assume that the perpendicular velocity is zero at a previous time step, then the perpendicular velocity at a current time step is equal in magnitude to the acceleration in the *y* direction (since it is 1-Hz data).

The validity of the projection algorithm for storms that have both velocity and total acceleration data (i.e., post 2012) is evaluated in Fig. A2 which shows the comparisons for Hurricanes Ian (2022) and Teddy (2020). For both storms, the acceleration in the *y* direction (sway or side–side) shows a strong correlation (both at $r = 0.99$) between the estimated accelerations using the algorithm and the measured accelerations from the accelerometer (Figs. A2a,d). In the *x* direction, for both storms, there were a significant amount of times where the accelerometers reported small accelerations, but the algorithm reported much higher magnitudes (Figs. A2b,e). The source of this error was traced to aircraft turns. In the dataset, turns were defined as times when the 5-s mean roll angle was greater than 0.1 rad and the heading rate was greater than 0.035 rad $s^{-1}$. This was subjectively verified to represent turns using aircraft position data (not shown). Since we could not find a way to overcome these errors, we eliminated aircraft turns from the analysis. Of note, eliminating locations identified as turns should not eliminate locations with high turbulence since turns typically occur at end points of legs where turbulence is minimal. With turns eliminated, the performance of the algorithm on accelerations in the *x* direction is substantially improved (Figs. A2c,f; $r = 0.72$ vs $r = 0.6$ in Hurricane Ian and $r = 0.82$ vs $r = 0.53$ in Hurricane Teddy). While not as strong of a fit as for accelerations in the *y* direction, this algorithm captures the general trend and allows us to explore all data between 2004 and 2012. Data prior to 2004 had a different format and did not report any vertical acceleration. Thus, it was not usable in this analysis. However, we were specifically able to obtain data from missions into Hurricanes Allen (1980) and Hugo (1989) from Neal Dorst at HRD, who reprocessed those data from stored magnetic tapes.

***Defining a bumpiness metric.*** To construct a bumpiness index, we tested many different groupings of the acceleration and jerk variables. The final bumpiness index is given in Eq. (A3):

$$B = \left\{ \left[ \left| a_X \right| + \left( \left| j_X \right| \times dt \right) \right] \times \left[ \left| a_y \right| + \left( \left| j_y \right| \times dt \right) \right] \times \left[ \left| a_Z \right| + \left( \left| j_z \right| \times dt \right) \right] \right\}^{1/3}. \tag{A3}$$

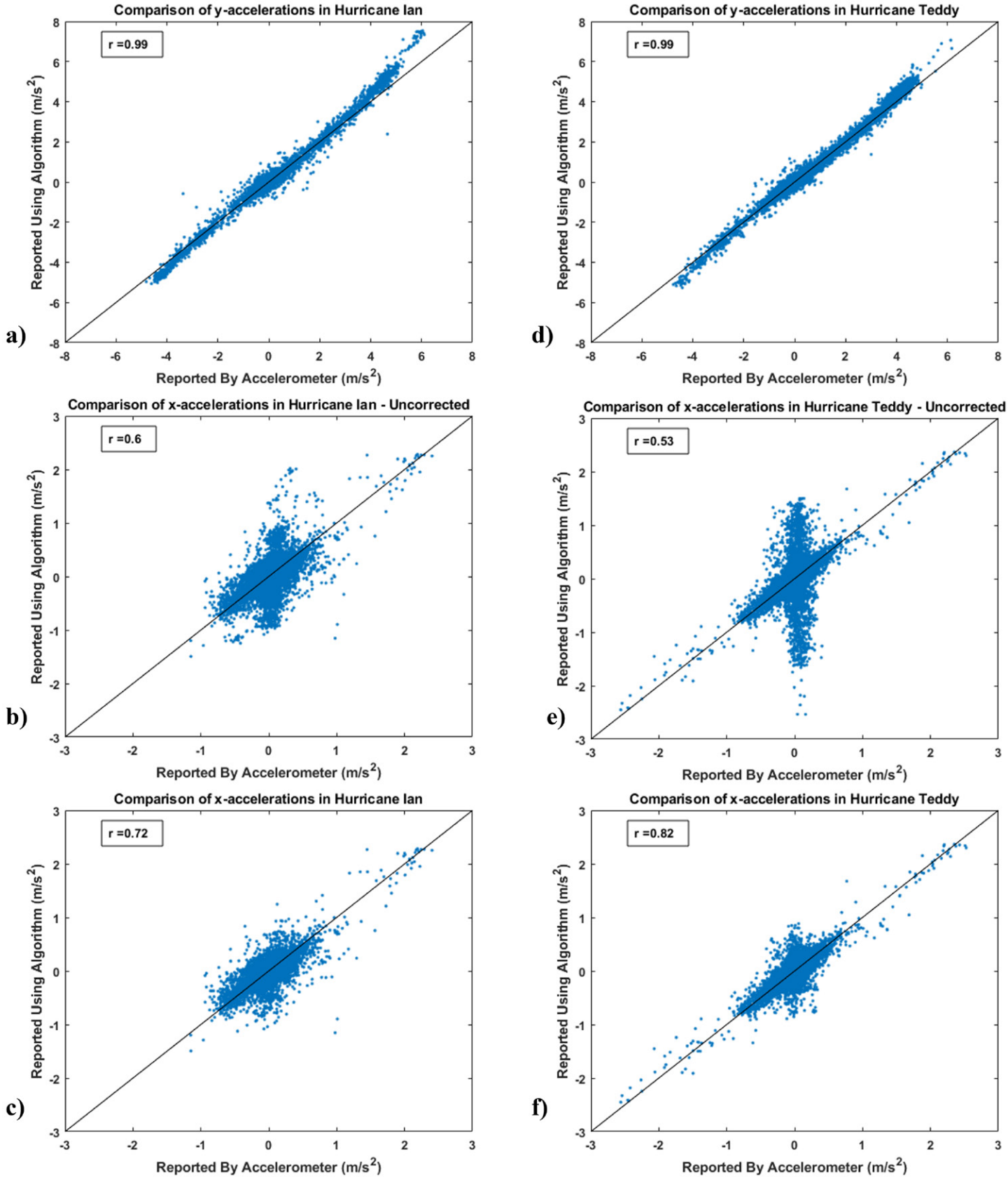


FIG. A2. A comparison for Hurricane Ian between estimated and measured (a) *y* accelerations, (b) *x* accelerations, and (c) *x* accelerations at points without turns. (d)–(f) As in (a)–(c), but for Hurricane Teddy.

In Eq. (A3), $dt$ is the time step (1 s with this dataset); $a_x$, $a_y$, and $a_z$ are the total accelerations in the $x$, $y$, and $z$ directions, respectively; and $j_x$, $j_y$, and $j_z$ are the total jerk in the $x$, $y$, and $z$ directions, respectively. Of note, as defined in the previous section, all the aircraft motion

estimates have implied temporal filters applied to their estimates. An absolute value is used since we want to quantify the combined effects of acceleration and jerk, and opposite signs can cancel out effects that are physically felt by people on the plane. The bumpiness output is in meters per square second, which is a mass-normalized time derivative of momentum.

Equation (A3) is the preferred equation for bumpiness because it gives equal weight to each axis. For example, a doubling of the first term, which is bumpiness in the *x* direction, leads to a doubling of the entire equation within the brackets. Further, a strength of Eq. (A3) is that if one term is zero, it does not influence the other terms. For example, another attempted equation for bumpiness is given in Eq. (A4). While this equation still has groups of terms for the *x*, *y*, and *z* directions and results in a bumpiness with units of meters per square second, the multiplication of terms produces a problem. A plane turning at a constant rate will have a nonzero $a_y$, but $j_y$ would be zero. In Eq. (A4), this would make the $\left(a_y \times j_y \times dt\right)$ term be equal to zero, even though someone on the aircraft would feel the effects of the turn. Another example is Eq. (A5), which was the first version of the equation tried. In Eq. (A5), the grouping of terms leads to an acceleration vector and a jerk vector. While the grouping of terms is done classically via the Pythagorean theorem, Eq. (A5) did not weigh changes to each term equally since the terms in the *z* direction are almost always significantly larger than in the *x* and *y* directions, and humans are more sensitive to smaller accelerations in the *x* and *y* directions than in the *z* direction (e.g., Benson et al. 1986; MacNeilage et al. 2010; Roditi and Crane 2012; Zaichik et al. 1999; Valko et al. 2012; Nesti et al. 2014). Using this equation, a doubling of the accelerations and jerk in the *y* direction would not significantly change the resulting bumpiness. The result was a term that quasi-represented vertical processes only and was not too different from quantifying vertical *g* forces. With the goal of representing the three-dimensional aspects of turbulence, neither of these equations are ideal:

$$B1_{\text{old}} = \left[\left(\left|a_X\right| \times \left|j_X\right| \times dt\right)^{1/2} + \left(\left|a_y\right| \times \left|j_y\right| \times dt\right)^{1/2} + \left(\left|a_Z\right| \times \left|j_z\right| \times dt\right)^{1/2}\right], \tag{A4}$$

$$B2_{\text{old}} = \left(a_X^2 + a_y^2 + a_Z^2\right)^{1/2} + \left[\left(j_X \times dt\right)^2 + \left(j_y \times dt\right)^2 + \left(j_z \times dt\right)^2\right]^{1/2}. \tag{A5}$$

## References


Aberson, S. D., M. T. Montgomery, M. Bell, and M. Black, 2006: Hurricane Isabel (2003): New insights into the physics of intense storms. Part II: Extreme localized wind. *Bull. Amer. Meteor. Soc.*, **87**, 1349–1354, https://doi.org/10.1175/BAMS-87-10-1349.

——, J. A. Zhang, and K. N. Ocasio, 2017: An extreme event in the eyewall of Hurricane Felix on 2 September 2007. *Mon. Wea. Rev.*, **145**, 2083–2092, https://doi.org/10.1175/MWR-D-16-0364.1.

Bass, E. J., 2002: Turbulence assessment and decision-making in commercial aviation: Investigating the current state of practice and the effects of technology interventions. *Int. J. Appl. Aviat. Stud.*, **2**, 11–22.

Benson, A., M. Spencer, and J. Stott, 1986: Thresholds for the detection of the direction of whole-body, linear movement in the horizontal plane. *Aviat. Space Environ. Med.*, **57**, 1088–1096.

Cangialosi, J. P., and R. Berg, 2021: Tropical cyclone report: Hurricane Delta (AL262020), 4–10 October 2020. NHC Tech. Rep., 46 pp., https://www.nhc.noaa.gov/data/tcr/AL262020_Delta.pdf.

Chan, W., 1995: An evaluation of real-time aviation turbulence metrics. M.S. thesis, Dept. of Meteorology, San Jose State University, ProQuest Dissertations Publishing, 105 pp.

Cione, J. J., and Coauthors, 2020: Eye of the storm: Observing hurricanes with a small unmanned aircraft system. *Bull. Amer. Meteor. Soc.*, **101**, E186–E205, https://doi.org/10.1175/BAMS-D-19-0169.1.

Cornman, L. B., C. S. Morse, and G. Cunning, 1995: Real-time estimation of atmospheric turbulence severity from in-situ aircraft measurements. *J. Aircr.*, **32**, 171–177, https://doi.org/10.2514/3.46697.

DeMaria, M., M. Mainelli, L. K. Shay, J. A. Knaff, and J. Kaplan, 2005: Further improvements to the Statistical Hurricane Intensity Prediction Scheme (SHIPS). *Wea. Forecasting*, **20**, 531–543, https://doi.org/10.1175/WAF862.1.

de Winkel, K. N., F. Soyka, and H. H. Bülthoff, 2020: The role of acceleration and jerk in perception of above-threshold surge motion. *Exp. Brain Res.*, **238**, 699–711, https://doi.org/10.1007/s00221-020-05745-7.

Dorst, N. M., 2007: The National Hurricane Research Project: 50 years of research, rough rides, and name changes. *Bull. Amer. Meteor. Soc.*, **88**, 1566–1588, https://doi.org/10.1175/BAMS-88-10-1566.

Eastin, M. D., W. M. Gray, and P. G. Black, 2005a: Buoyancy of convective vertical motions in the inner core of intense hurricanes. Part I: General statistics. *Mon. Wea. Rev.*, **133**, 188–208, https://doi.org/10.1175/MWR-2848.1.

——, ——, and ——, 2005b: Buoyancy of convective vertical motions in the inner core of intense hurricanes. Part II: Case studies. *Mon. Wea. Rev.*, **133**, 209–227, https://doi.org/10.1175/MWR-2849.1.

Evans, J. E., 1985: Weather radar studies. U.S. Dept. of Transportation Rep. DOT/FAA-PM-85-16, 48 pp.

Federal Aviation Administration, 2012: Aeronautical information manual: Official guide to basic flight information and ATC procedures. FAA Aeronautical Information Manual, 901 pp., https://www.faa.gov/air_traffic/publications/media/AIM_Basic_dtd_2-20-25_post.pdf.

Grant, P. R., and B. Haycock, 2008: Effect of jerk and acceleration on the perception of motion strength. *J. Aircr.*, **45**, 1190–1197, https://doi.org/10.2514/1.33757.

Jorgensen, D. P., E. J. Zipser, and M. A. LeMone, 1985: Vertical motions in intense hurricanes. *J. Atmos. Sci.*, **42**, 839–856, https://doi.org/10.1175/1520-0469(1985)042<0839:VMIIH>2.0.CO;2.

Lee, J. T., 1977: Application of Doppler weather radar to turbulence measurements which affect aircraft. Federal Aviation Administration Rep. FAA-RD-77-145, 52 pp., https://apps.dtic.mil/sti/tr/pdf/ADA048603.pdf.

Leise, J. A., and J. Masters, 2013: Wind measurement from aircraft, 1993: annotated and updated 2013. NOAA Tech. Memo. OAR ARL-266, 222 pp., https://doi.org/10.7289/V5/TM-OAR-ARL-266.

Lorsolo, S., J. A. Zhang, F. Marks, and J. Gamache, 2010: Estimation and mapping of hurricane turbulent energy using airborne doppler measurements. *Mon. Wea. Rev.*, **138**, 3656–3670, https://doi.org/10.1175/2010MWR3183.1.

MacCready, P. B., 1964: Standardization of gustiness values from aircraft. *J. Appl. Meteor.*, **3**, 439–449, https://doi.org/10.1175/1520-0450(1964)003<0439:SOGVFA>2.0.CO;2.

MacNeilage, P. R., M. S. Banks, G. C. DeAngelis, and D. E. Angelaki, 2010: Vestibular heading discrimination and sensitivity to linear acceleration in head and world coordinates. *J. Neurosci.*, **30**, 9084–9094, https://doi.org/10.1523/JNEUROSCI.1304-10.2010.

Marks, F. D., P. G. Black, M. T. Montgomery, and R. W. Burpee, 2008: Structure of the eye and eyewall of Hurricane Hugo (1989). *Mon. Wea. Rev.*, **136**, 1237–1259, https://doi.org/10.1175/2007MWR2073.1.

Martinez, J., M. M. Bell, J. L. Vigh, and R. F. Rogers, 2017: Examining tropical cyclone structure and intensification with the FLIGHT+ dataset from 1999 to 2012. *Mon. Wea. Rev.*, **145**, 4401–4421, https://doi.org/10.1175/MWR-D-17-0011.1.

Melnikov, V. M., and R. J. Doviak, 2009: Turbulence and wind shear in layers of large Doppler spectrum width in stratiform precipitation. *J. Atmos. Oceanic Technol.*, **26**, 430–443, https://doi.org/10.1175/2008JTECHA1108.1.

Nesti, A., M. Barnett-Cowan, P. R. Macneilage, and H. H. Bülthoff, 2014: Human sensitivity to vertical self-motion. *Exp. Brain Res.*, **232**, 303–314, https://doi.org/10.1007/s00221-013-3741-8.

NOAA, 2024: Tropical cyclone climatology. https://www.nhc.noaa.gov/climo/.

Pincus, R., and Coauthors, 2021: Observations from the NOAA P-3 aircraft during ATOMIC. *Earth Syst. Sci. Data*, **13**, 3281–3296, https://doi.org/10.5194/essd-13-3281-2021.

Roditi, R. E., and B. T. Crane, 2012: Directional asymmetries and age effects in human self-motion perception. *J. Assoc. Res. Otolaryngol.*, **13**, 381–401, https://doi.org/10.1007/s10162-012-0318-3.

Schwartz, B., 1996: The quantitative use of PIREPs in developing aviation weather guidance products. *Wea. Forecasting*, **11**, 372–384, https://doi.org/10.1175/1520-0434(1996)011<0372:TQUOPI>2.0.CO;2.

Sharman, R., C. Tebaldi, G. Wiener, and J. Wolff, 2006: An integrated approach to mid- and upper-level turbulence forecasting. *Wea. Forecasting*, **21**, 268–287, https://doi.org/10.1175/WAF924.1.

Sharman, R. D., L. B. Cornman, G. Meymaris, J. Pearson, and T. Farrar, 2014: Description and derived climatologies of automated in situ eddy-dissipation-rate reports of atmospheric turbulence. *J. Appl. Meteor. Climatol.*, **53**, 1416–1432, https://doi.org/10.1175/JAMC-D-13-0329.1.

Storer, L. N., P. D. Williams, and M. M. Joshi, 2017: Global response of clear-air turbulence to climate change. *Geophys. Res. Lett.*, **44**, 9976–9984, https://doi.org/10.1002/2017GL074618.

Tvaryanas, A. P., 2003: Epidemiology of turbulence–related injuries in airline cabin crew, 1992–2001. *Aviat. Space Environ. Med.*, **74**, 970–976.

Valko, Y., R. F. Lewis, A. J. Priesol, and D. M. Merfeld, 2012: Vestibular labyrinth contributions to human whole-body motion discrimination. *J. Neurosci.*, **32**, 13 537–13 542, https://doi.org/10.1523/JNEUROSCI.2157-12.2012.

Wunsch, K. E. D., and A. C. Didlake, 2018: Analyzing tropical cyclone structures during secondary eyewall formation using aircraft in situ observations. *Mon. Wea. Rev.*, **146**, 3977–3993, https://doi.org/10.1175/MWR-D-18-0197.1.

Zaichik, L., V. Rodchenko, I. Rufov, Y. Yashin, and A. White, 1999: Acceleration perception. *AIAA Modeling and Simulation Technologies Conference—A Collection of Technical Papers*, Portland, OR, American Institute of Aeronautics and Astronautics, 512–520, https://arc.aiaa.org/doi/abs/10.2514/6.1999-4334.

Zhang, J. A., F. D. Marks, M. T. Montgomery, and S. Lorsolo, 2011: An estimation of turbulent characteristics in the low-level region of intense Hurricanes Allen (1980) and Hugo (1989). *Mon. Wea. Rev.*, **139**, 1447–1462, https://doi.org/10.1175/2010MWR3435.1.